

Article

Multivariate Analysis of Laser-Induced Tissue Ablation: Ex Vivo Liver Testing

Suhyun Park¹ and Hyun Wook Kang^{2,*}

¹ School of Electrical and Electronics Engineering, Chung-Ang University, Seoul 06974, Korea; suhyun@cau.ac.kr

² Department of Biomedical Engineering and Center for Marine-Integrated Biomedical Technology (BK 21 Plus), Pukyong National University, Busan 48513, Korea

* Correspondence: wkang@pukyong.ac.kr; Tel.: +82-51-629-5774

Received: 8 September 2017; Accepted: 20 September 2017; Published: 22 September 2017

Abstract: A number of laser parameters are often regulated to enhance ablation efficiency during laser surgery. As one of clinical treatments, laser removal of benign prostate hyperplasia has been well accepted by surgical urologists. However, due to complex interactions of the surgical parameters, the procedure is still lengthy and dependent upon the surgeon's skill and experience. The aim of the current study is to evaluate the feasibility of response surface method (RSM) to comprehend ablative interactions of multi-parameters and to identify the optimal ablation rate (AR). As a surrogate model in the feasibility study, bovine liver tissue was utilized for ex vivo ablation testing. Three laser parameters pertinent to laser prostatectomy were selected: power (P), treatment speed (TS), and beam spot (BS). As a three-level fractional factorial RSM, Box Behnken design (BBD) was employed to identify the range of each parameter for achieving the optimal AR. The results showed that regardless of TS, AR was linearly contingent on both P and BS due to high irradiance. TS of 6~7 mm/s induced the maximal AR when P of 180 W and BS of 0.4 mm². The corresponding volumetric density energy yielded an ablation volume of 80 mm², which was close to a transition to volumetric saturation. The BBD-based model showed a good agreement with the experimental data in terms of ablation volume. The proposed multivariate parametric analysis can be an efficient design method to identify the optimal conditions for laser therapeutics. Further investigations will be performed on prostatic tissue to validate the proposed approach and to explore various optimization processes.

Keywords: ablation rate; Box–Behnken design; volumetric energy density; response surface method

1. Introduction

For decades, therapeutic laser systems have been developed and successfully employed for clinical applications in various fields such as dentistry, ophthalmology, and urology [1]. In order to achieve efficient tissue removal and minimal thermal injury, a number of laser parameters have been evaluated, including wavelength, pulse duration, energy/power, and beam size [1,2]. In addition, a variety of surgical parameters have been investigated in terms of movement technique, repetition, and irradiation time for maximizing ablation outcomes [1,3]. However, due to complex interactions among the parameters, laser-induced tissue ablation still requires rigorous testing to identify the optimal conditions and eventually to ensure efficacy and safety during laser treatment.

One successful laser treatment is vaporization of benign prostate hyperplasia (BPH), also called laser prostatectomy. Symptomatic BPH is one of urological diseases that occur to men aged 40 years or older [4,5]. Excessive growth of stromal tissue in the peripheral zone of the prostate causes obstruction of urination, eventually leading to dysuria, nocturia, and frequent urge [4,6]. Other than medications that merely suppress the enlargement of the prostate, a number of surgical treatments have been developed to treat BPH, such as radiofrequency (transurethral resection of the prostate; TURP), laser,

microwave, and high intensity focused ultrasound (HIFU) [7,8]. Among various methods, the laser prostatectomy has widely been accepted by surgical urologists due to hemostatic and rapid tissue removal and low complications [9]. During the laser prostatectomy, urologists typically insert an optical fiber through the urethra to deliver high laser power and then maneuver the fiber to remove prostatic tissue. Thus, various surgical parameters, such as laser power, fiber size, working distance, and movement speed, are simultaneously regulated to achieve favorable clinical outcomes [3,10,11]. In particular, the laser power has recently been increased to treat large prostate glands (>80 cc) and eventually to reduce the procedure time [12]. However, the efficacy of the laser prostatectomy is still contingent upon the surgeon's skills, which needs more systematic approaches to optimize the surgical parameters and to attain more effective laser prostatectomy. In fact, most surgical urologists are still dependent upon their clinical experience to select the treatment parameters. Thus, the multivariate optimization of the surgical parameters is still necessary to reveal favorable treatment conditions and eventually to provide quantitative training for the laser prostatectomy.

In order to improve laser-induced ablation process, design of experiments (DOE) can be used to determine the optimal settings for the critical factors in the tissue ablation [13]. Through DOE, by selecting factors and levels that affect the performance of the ablation process, one can investigate the effect of each factor at more than one setting. A full factorial design is the most common experimental design when the purpose is to determine the critical factors and the range of the values in the study. It can evaluate every possible combination between all the factors. With an increase of a number of factors, the number of experiments in the full factorial design increases exponentially. Instead, a fractional factorial can be employed to acquire information of interactions with fewer experiments. The simplest assumption for the factorial design is the two-level approach, which assumes that there are only two levels for each factor in the natural linear process. In order to fit the output responses in a curved response surfaces, response surface method (RSM) uses additional points that can help estimate the higher-order interactions [14]. Central composite designs (CCD) and Box–Behnken designs (BBD) are the most widely used RSM design [14,15]. CCD is for fitting quadratic response surfaces by employing extra levels including the center point in addition to the two-level full-factorial. On the other hand, BBD is a three-level fractional factorial RSM design for fitting the second-order response surfaces, which is mostly useful when extreme treatment combinations are required to avoid.

The purpose of the current research was to investigate the feasible application of RSM to reveal ablative interactions of multi-parameters and to optimize surgical parameters for the maximum tissue ablation efficiency. It was hypothesized that the statistical approach could not only reduce the number of tests but also could explore the optimal conditions for laser therapeutics. Due to easy procurement and tissue abundance, bovine liver was used as a surrogate model for the current feasibility study. Multivariate analysis with three-level BBD was employed to comprehend individual or interactive effects of various ablation parameters. Ex vivo tissue removal was investigated in light of three surgical variables for identifying the optimal ablation conditions.

2. Methods

In order to apply BBD for tissue ablation, three laser parameters were selected: power (P), treatment speed (TS), and beam size (BS). The selected parameters were considered significant factors that could affect clinical outcomes of laser prostatectomy. Using the three laser parameters, BBD was implemented to optimize the rate of tissue removal. Since it is desirable to avoid the extreme values for the three variables (P, TS, and BS) in the ablation process, BBD was a preferred method, compared with CCD [14]. Table 1 shows the coded factor levels for BBD for three-level and three-variable system. The levels of +1, −1, and 0 mean the high, low, and middle values, respectively. Two-level full factorial was repeated three times for two factors (i.e., levels of +1 and −1) while keeping one factor at the middle value (i.e., level of 0). For example, the first set of four points in Table 1 was to keep BS at the middle value with two-level full factorials for P and TS. Then, P and TS were set at the middle value in that order. Lastly, the center points (C) were added to provide stability and to estimate curvature.

Generally, three-factor BBD uses three center points. Thus, the total number of the sample points was 15. The selected samples in the BBD are displayed in Figure 1a. The samples are at the center of the edges and in the center of the design space.

Table 1. Coded factor levels for Box–Behnken design for three-variable system

Rank	P *	TS *	BS *
1	−1	−1	0
2	1	−1	0
3	−1	1	0
4	1	1	0
5	−1	0	−1
6	1	0	−1
7	−1	0	1
8	1	0	1
9	0	−1	−1
10	0	1	−1
11	0	−1	1
12	0	1	1
C **	0	0	0
C	0	0	0
C	0	0	0

* P = power, TS = treatment speed, and BS = beam size, ** C = central point.

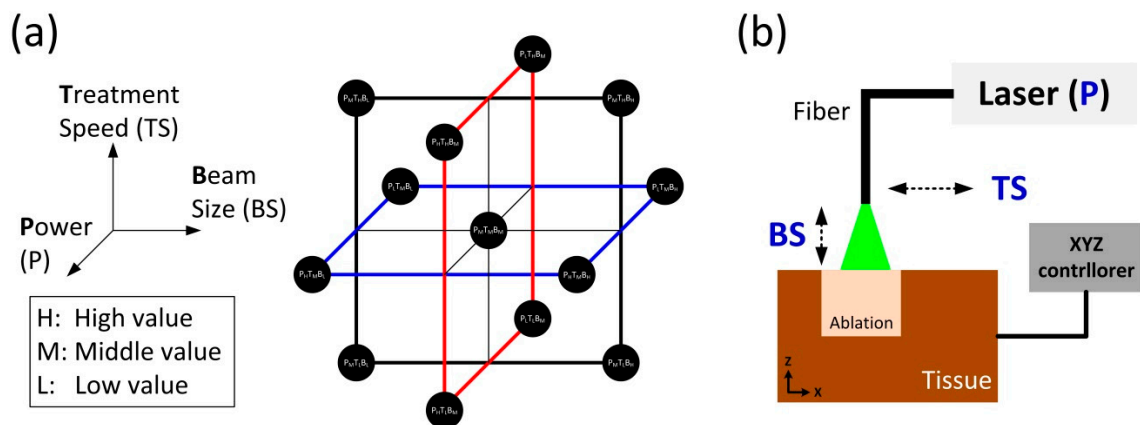


Figure 1. Schematic illustration of parametric analysis: (a) Box–Behnken Design (BBD); (b) experimental setup for laser-induced tissue ablation.

Figure 1b shows an experimental setup of ex vivo laser-induced tissue ablation. For the current feasibility study, bovine liver tissue was selected as a surrogate model due to easy procurement and abundance. Unlike prostatic tissue, the liver tissue could be sufficiently prepared for a wide range of repeated tests. In spite of different optical properties, the bovine liver could thus be the proper sample for the initial testing particularly to reduce the number of test conditions. The liver tissue was procured from a local slaughterhouse. All the samples were prepared in a size of $2 \times 2 \text{ cm}^2$ and stored at $4 \text{ }^\circ\text{C}$ in saline to prevent any dehydration and structural deformation prior to laser testing. Each specimen was placed in a tissue holder and covered with a metal plate containing a rectangular aperture ($1 \times 1 \text{ cm}^2$). Thus, the tissue surface exposed through the aperture was merely ablated during the irradiation. A motion controller was used to manipulate the movement of the tissue holder along the x - y - z directions. The controller thereby determined both beam size (distance-dependent) and treatment speed. A customized quasi-Q-switched 532 nm laser system was employed to irradiate high power laser light on the tissue surface and to achieve photothermal ablation. A 600- μm multi-mode optical

fiber (flat-ended; NA = 0.22) was used to deliver the laser light to the targeted tissue. The physical distance between the fiber tip and the tissue surface regulated various beam spot sizes. During the tissue ablation, saline was supplied to the irradiated spot at 5.6 mL/min for convective cooling and fiber tip cleaning to emulate clinical situations. Table 2 summarizes three-level values of each parameter for ablation experiments. As clinical laser systems can deliver power levels ranging from 120 to 200 W, the three values (120, 160, and 200 W) were selected for P [12]. Based upon previous studies and clinical conditions, the three values for TS and BS were chosen, respectively [3,9,16]. According to Figure 1a, the three levels for each parameter included low, middle, and high values. Based upon TS, the total irradiation times were determined as 10, 2, and 1.1 s for 1, 5, and 9 mm/s, respectively. Each condition was independently tested five times (N = 5) by following the BBD plans as shown in Figure 1a.

Table 2. Three-level values of each parameter for experimental matrix.

Parameter	Low Value (−1)	Middle Value (0)	High Value (+1)
Power (P)	120 W	160 W	200 W
Treatment Speed (TS)	1 mm/s	5 mm/s	9 mm/s
Beam Size (BS)	0.4 mm ²	1.1 mm ²	1.8 mm ²

Figure 2 illustrates post-experimental analysis on ablated bovine tissues. Each specimen was vertically cross-sectioned along *y*-axis by 1-mm thickness (*dt*). A total of 10 cross-sections were prepared, and a digital camera was used to photograph all the cross-sections (i.e., *y*-*z* plane). Image J (National Institute of Health, Bethesda, MD, USA) was then implemented to detect the boundary of each ablated crater in the acquired image and to estimate the detected area (*A_i*). Ten quantified areas (i.e., *A₁*~*A₁₀*) were integrated in terms of the cross-section thickness (*dt*) to estimate ablation volume (mm³) for each condition. The corresponding ablation rate (AR; mm³/s) was also calculated by dividing the ablation volume by a total irradiation time. Minitab (Minitab 17, State Collage, PA, USA) was also used to implement a response surface method and to assess the effect of all the parameters on ablation efficiency for eventually determining the optimal therapeutic conditions. For statistical analysis, analysis of variance (ANOVA) was performed, and *p* < 0.05 was considered significant.

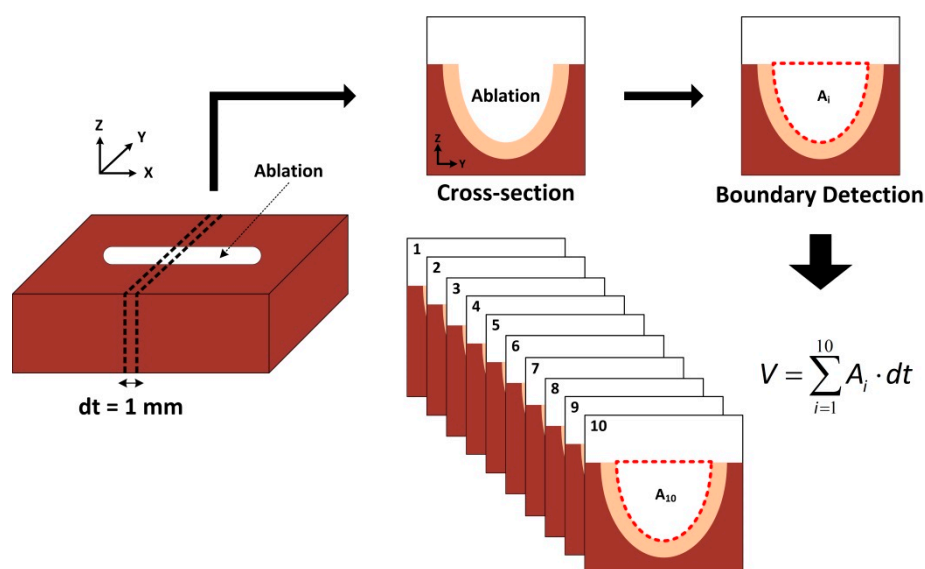


Figure 2. Schematic illustration of volume quantification on ablated tissue (*dt*: tissue thickness, *A*: ablated area, and *V*: estimated ablation volume).

3. Results and Discussion

Figure 3 demonstrates cross-sectional images of the liver tissue ablated at various conditions; (a) constant P of 160 W; (b) constant TS of 5 mm/s; and (c) constant BS of 1.1 mm². The tissue section represents the central vertical cross-section. In the case of constant P, significantly more tissue ablation ($20.9 \pm 3.3 \text{ mm}^2$) occurred with slower TS and smaller BS (left image; Figure 3a) due to higher irradiance along with longer interaction time (i.e., 400 W/mm^2 and 10 s for left image). On the other hand, the highest TS and the largest BS resulted in relatively smaller irradiance (89 W/mm^2) and shorter interaction time (1 s), leading to superficial tissue ablation ($3.2 \pm 0.3 \text{ mm}^2$ for right image; $p < 0.05$). Thus, it was noted that both TS and BS were deterministic factors for tissue ablation. Figure 3b demonstrated that for constant TS, the degree of tissue removal (6.9 ± 0.8 , 6.5 ± 0.6 , and $5.3 \pm 0.7 \text{ J/mm}^2$ for left, middle, and right images, respectively) increased in the order of irradiance (i.e., 300, 145, and 111 W/mm^2 for left, middle, and right images, respectively). However, compared to Figure 3a, the increase rate of the tissue ablation was relatively less evident (6.5-fold for Figure 3a vs. 1.3-fold for Figure 3b), implicating that in spite of constant TS, the variations in other parameters (P and BS) could interactively compensate ablation efficiency. Lastly, constant BS in Figure 3c showed that the ablation efficiency increased with decreasing TS and increasing P. In spite of 40% lower irradiance (109 W/mm^2), the left image showed almost two-fold enhancement in the ablated area ($12.4 \pm 4.4 \text{ mm}^2$; $p < 0.05$), compared with the right image ($6.8 \pm 0.8 \text{ mm}^2$ and 180 W/mm^2). TS was thus more deterministic than P on the ablation efficiency, given the constant values of BS. Therefore, according to Figure 3, three parameters interactively affected the degree of tissue removal particularly after application of high laser power.

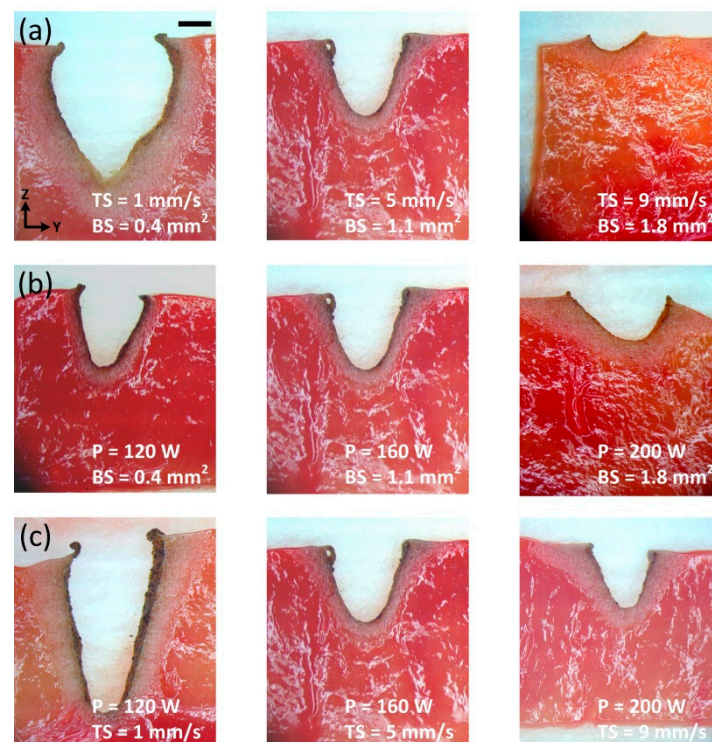


Figure 3. Images of ablated tissue at various testing conditions: (a) constant power (160 W); (b) constant treatment speed (5 mm/s); (c) constant beam size (1.1 mm²). Bar = 1 mm.

To investigate parametric effects of P, TS, and BS on ablation efficiency, BBD was performed. Figure 4 exhibits parametric analysis on AR as a function of P, TS, and BS. Two parameters were evaluated simultaneously while another parameter was fixed (fixed parameters: (a) TS; (b) BS; and (c) P). The upper images represented a low value of the fixed parameter whereas the lower images showed a high value of the fixed one. In the case of the fixed TS (Figure 4a), both the high and

the low values demonstrate that AR was maximized at P ranging between 180 and 200 W and BS of 0.4 mm². Thus, AR was linearly contingent upon both P (proportional) and BS (inversely proportional) at the fixed TS, in that high P and low BS can result in high irradiance. Figure 4b with the fixed BS presents that AR was still maximized at P of 180~200 W, which was similar to Figure 4a. However, the optimal TS ranged between 6 and 7 mm/s, which was quite larger than the low value of TS (1 mm/s; longer irradiation time). The current finding implies that longer interaction time (i.e., slower TS) was hardly necessary to maximize AR. In fact, the beam divergence from the fiber could reduce the irradiance lower than ablation threshold as the ablation crater became deeper. Furthermore, clinical laser prostatectomy considers both the amount of tissue removal and the total lasing time equally significant. Lastly, Figure 4c exhibits that for both high and low values of P, AR was maximized at BS of 0.4 mm² and TS of 6~7 mm/s, which was comparable to Figure 4a,b.

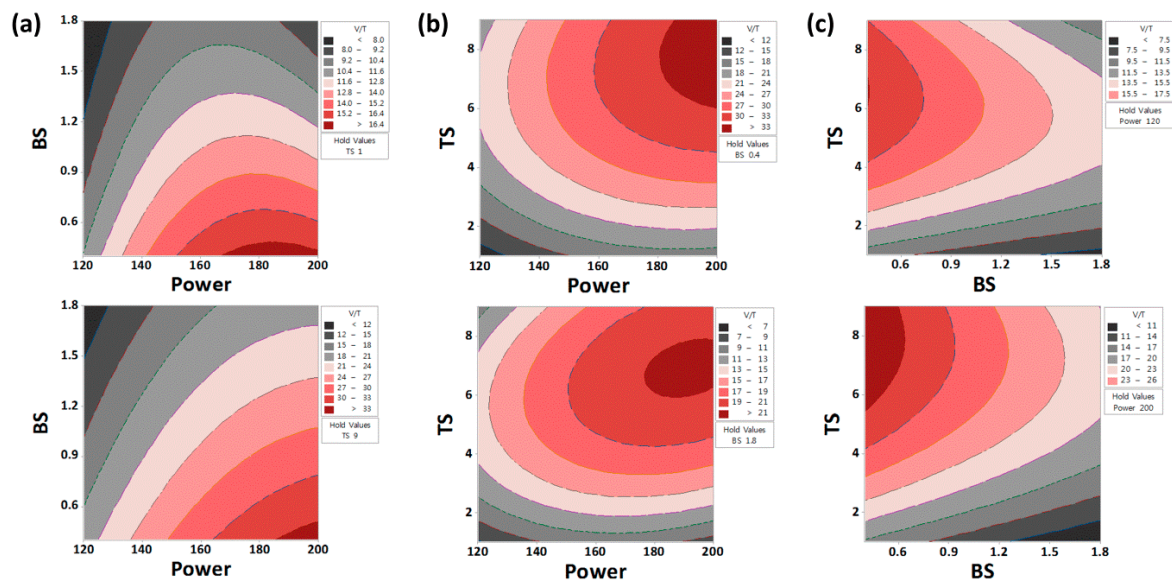


Figure 4. Parametric analysis on ablation rate (mm³/s) with fixed parameters: (a) treatment speed (TS); (b) beam size (BS); (c) power (P).

In an attempt to assess collective effects of laser parameters, laser-induced ablation volume was quantified as a function of volumetric energy density ($VED = P/[TS \times BS]$; J/mm³) as shown in Figure 5. Since VED represents the amount of laser energy that was used to remove 1 mm³ of tissue, the correlation between the ablation volume and VED could evaluate the overall ablation efficiency. According to Figure 5, the BBD model was validated by using the experimental data, in that a comparable tendency was found in the variations in ablation volume ($p = 0.36$). Regardless of the data sets, the ablation volume initially increased with VED but became saturated at higher VEDs. As the maximum ablation volume of 209 mm³ occurred at VED of 400 J/mm³, the highest VED should be selected to merely maximize the total tissue removal by increasing P and/or decreasing both TS and BS. Although VED effectively described the overall variations in the ablation volume, the increase rate (i.e., slope) of the ablation volume suddenly decreased at around 100 J/mm³. Furthermore, to shorten laser prostatectomy times, particularly for treating large prostate glands, AR could be a more crucial factor for optimization of the ablation conditions.

According to the current BBD results, the optimal VED ranged from 71 (P = 200 W, TS = 7 mm/s, and BS = 0.4 mm²) to 75 J/mm³ (P = 180 W, TS = 6 mm/s, and BS = 0.4 mm²). Thus, the corresponding ablation volume was approximately 80 mm³ (Figure 5). It can be conceived that the optimal parameters for laser prostatectomy could be identified prior to the onset of volumetric saturation in tissue (i.e., maximizing P and TS and minimizing BS). Both P and BS yielded a linear correlation with AR, in that the two parameters can determine the spatial distribution of power on the tissue surface

(i.e., irradiance). On the other hand, TS showed a non-linear (i.e., parabolic) correlation with AR, implicating that due to beam divergence and the resultant irradiance, the interaction time between laser and tissue should be optimized to achieve high ablation efficiency. In addition, unlike P and BS that are typically determined by laser system and optical fiber (device-dependent), TS is controlled by urologists during laser prostatectomy (surgeon-dependent) [16,17]. Thus, the training on fiber movement during laser treatment would be instrumental in attaining better clinical outcomes [3]. However, the current study merely focused on ablation efficiency rather than safety. In order to enhance clinical results, the degree of tissue coagulation should additionally be considered during BBD analysis as thermal injury in tissue considerably determines wound healing after laser prostatectomy. Moreover, liver tissue was tested for the current study, which hardly reflects fibrous prostatic tissue. Thus, further BBD investigations on canine prostate models will be pursued to identify the optimal surgical parameters by considering blood perfusion, tissue denaturation, and chronic healing response. In-depth parametric optimization may further ensure efficacy and safety of laser prostatectomy for BPH patients.

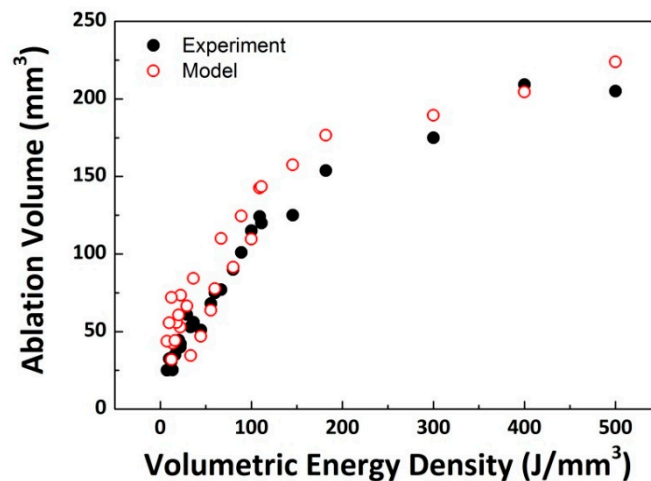


Figure 5. Collective effect of volumetric energy density (J/mm^3) on laser-induced ablation volume.

The purpose of the current study was to identify the maximal ablation rate to facilitate laser prostatectomy on large prostate glands (>80 cc) for clinical translation. According to Figure 5, a higher VED yielded a larger removal of tissue. For instance, at the VED of $500 \text{ J}/\text{mm}^3$, the corresponding AR is $20.5 \text{ mm}^3/\text{s}$ (=ablation volume of 205 mm^3 /irradiation time of 10 s). On the other hand, the optimal VED found in this study was estimated to be $75 \text{ J}/\text{mm}^3$ (Figure 4), which resulted in almost $50 \text{ mm}^3/\text{s}$ (= $80 \text{ mm}^3/1.7 \text{ s}$). Although the difference in the ablation volume between the maximal and the optimal VEDs (i.e., 500 vs. $80 \text{ J}/\text{mm}^3$) was 2.6-fold, the optimal VED could yield 140% faster removal of tissue due to shorter interaction times. Given the same irradiation time, the optimal VED could ablate more tissue due to high AR. In clinical situations, the typical size of large prostates for BPH treatment ranges from 80 to 120 cc [12]. Based upon the current findings, surgical urologists can remove 100 cc of prostate in around 34 min at the optimal VED while removing the same size in approximately 80 min at the maximal VED. However, it should be noted that the average clinical procedure for a 100 cc prostate gland takes around 120 min, which is 1.5–3.5 times long as the estimated procedure times [12]. One of the explanations could [18] be tissue component. Unlike BPH consisting of stromal tissue [6], the liver is glandular tissue, which is relatively easy to ablate and can thus be associated with a lower ablation threshold (i.e., high AR). Furthermore, optical properties of the liver are greatly different from those of prostate. For instance, the absorption coefficient of the liver at 532 nm is 4.5-fold higher than that of the prostate (i.e., 10.9 cm^{-1} for liver vs. 2.4 cm^{-1} for prostate [18]). Although easy and abundant procurement of the liver tissue was quite beneficial for the current feasibility testing,

the tissue properties could substantially affect the ablative tissue responses. Another explanation is the progress of thermal denaturation of the collagen in the prostatic tissue, which is thermo-mechanically resistant to the laser ablation process. Further investigations on collagenous tissue are currently underway in order to compare with the current findings. Specifically, two consecutive tests with (1) bull/canine prostate and (2) cadaveric human prostate will be conducted to validate the proposed parametric analysis for clinical translation in terms of ablation efficiency.

4. Conclusions

The current multivariate analysis demonstrated parametric approaches to determine the optimal ablation conditions for laser prostatectomy. Due to linear and quadratic effects of laser parameters, three-level BBD design was able to identify the parameter values (180~200 W, 6~7 mm/s, and 0.4 mm²) for the maximal AR. For clinical translation into laser prostatectomy, the proposed parametric analysis will be validated with fibrotic prostate tissue in terms of ablation efficiency. The application of three-level RSM design can be a feasible and simple way to identify the optimal ablation parameters for providing quantitative training for laser prostatectomy and eventually achieving better clinical outcomes.

Acknowledgments: This research was supported by a grant from Marine Biotechnology Program (20150220) funded by Ministry of Oceans and Fisheries, Korea.

Author Contributions: S.P. and H.W.K. conceived and designed experiments; S.P. analyzed the data and wrote the paper; H.W.K. conducted the experiments and wrote the paper.

Conflicts of Interest: The authors declare no conflict of interest.

References

1. Niemz, M.H. *Laser-Tissue Interactions: Fundamentals and Applications*; Springer: Berlin, Germany, 2004; pp. 151–247.
2. Vogel, A.; Venugopalan, V. Mechanisms of pulsed laser ablation of biological tissues. *Chem. Rev.* **2003**, *103*, 577–644. [[CrossRef](#)] [[PubMed](#)]
3. Muir, G.; Sancha, F.G.; Bachmann, A.; Choi, B.; Collins, E.; de la Rosette, J.; Reich, O.; Tabatabaei, S.; Woo, H. Techniques and Training with GreenLight HPS 120-W Laser Therapy of the Prostate: Position Paper. *Eur. Urol. Suppl.* **2008**, *7*, 370–377. [[CrossRef](#)]
4. Unnikrishnan, R.; Almassi, N.; Fareed, K. Benign prostatic hyperplasia: Evaluation and medical management in primary care. *Cleavel. Clin. J. Med.* **2017**, *84*, 53–64. [[CrossRef](#)] [[PubMed](#)]
5. Thangasamy, I.A.; Chalasani, V.; Bachmann, A.; Woo, H.H. Photoselective vaporisation of the prostate using 80-W and 120-W laser versus transurethral resection of the prostate for benign prostatic hyperplasia: A systematic review with meta-analysis from 2002 to 2012. *Eur. Urol.* **2012**, *62*, 315–323. [[CrossRef](#)] [[PubMed](#)]
6. Aaron, L.; Franco, O.E.; Hayward, S.W. Review of Prostate Anatomy and Embryology and the Etiology of Benign Prostatic Hyperplasia. *Urol. Clin. N.Am.* **2016**, *43*, 279–288. [[CrossRef](#)] [[PubMed](#)]
7. Miano, R.; De Nunzio, C.; Asimakopoulos, A.D.; Germani, S.; Tubaro, A. Treatment options for benign prostatic hyperplasia in older men. *Med. Sci. Monit* **2008**, *14*, RA94–RA102. [[PubMed](#)]
8. Darnell, S.E.; Hall, T.L.; Tomlins, S.A.; Cheng, X.; Ives, K.A.; Roberts, W.W. Histotripsy of the Prostate in a Canine Model: Characterization of Post-Therapy Inflammation and Fibrosis. *J. Endourol.* **2015**, *29*, 810–815. [[CrossRef](#)] [[PubMed](#)]
9. Malek, R.S.; Kang, H.W.; Coad, J.E.; Koullick, E. Greenlight photoselective 120-watt 532-nm lithium triborate laser vaporization prostatectomy in living canines. *J. Endourol.* **2009**, *23*, 837–845. [[CrossRef](#)] [[PubMed](#)]
10. Choi, B.; Tabatabaei, S.; Bachmann, A.; Collins, E.; de la Rosette, J.; Sancha, F.G.; Muir, G.; Reich, O.; Woo, H. GreenLight HPS 120-W Laser for Benign Prostatic Hyperplasia: Comparative Complications and Technical Recommendations. *Eur. Urol. Suppl.* **2008**, *7*, 384–392. [[CrossRef](#)]
11. Seitz, M.; Sroka, R.; Gratzke, C.; Schlenker, B.; Steinbrecher, V.; Khoder, W.; Tilki, D.; Bachmann, A.; Stief, C.; Reich, O. The Diode Laser: A Novel Side-Firing Approach for Laser Vaporisation of the Human Prostate—Immediate Efficacy and 1-Year Follow-Up. *Eur. Urol.* **2007**, *52*, 1717–1722. [[CrossRef](#)] [[PubMed](#)]

12. Rajih, E.; Tholomier, C.; Hueber, P.A.; Alenizi, A.M.; Valdivieso, R.; Azizi, M.; Gonzalez, R.R.; Eure, G.; Kritekman, L.; Hai, M.; et al. Evaluation of Surgical Outcomes with Photoselective GreenLight XPS Laser Vaporization of the Prostate in High Medical Risk Men with Benign Prostatic Enlargement: A Multicenter Study. *J. Endourol.* **2017**, *31*, 686–693. [[CrossRef](#)] [[PubMed](#)]
13. Eriksson, L.; Johansson, E.; Kettaneh-Wold, N.; Wikström, C.; Wold, S. *Design of Experiments*; Umeric Academy: Umea, Sweden, 2000; pp. 172–174.
14. Khuri, A.I.; Mukhopadhyay, S. Response surface methodology. *Wiley Interdiscip. Rev. Comput. Stat.* **2010**, *2*, 128–149. [[CrossRef](#)]
15. Ferreira, S.L.C.; Bruns, R.E.; Ferreira, H.S.; Matos, G.D.; David, J.M.; Brandão, G.C.; da Silva, E.G.P.; Portugal, L.A.; dos Reis, P.S.; Souza, A.S.; et al. Box-Behnken design: An alternative for the optimization of analytical methods. *Anal. Chim. Acta* **2007**, *597*, 179–186. [[CrossRef](#)] [[PubMed](#)]
16. Ko, W.J.; Choi, B.B.; Kang, H.W.; Rajabhandharaks, D.; Rutman, M.; Osterberg, E.C. Defining optimal laser-fiber sweeping angle for effective tissue vaporization using 180 W 532 nm lithium triborate laser. *J. Endourol.* **2012**, *26*, 313–317. [[CrossRef](#)] [[PubMed](#)]
17. Osterberg, E.C.; Kauffman, E.C.; Kang, H.W.; Koullick, E.; Choi, B.B. Optimal laser fiber rotational movement during photoselective vaporization of the prostate in a bovine ex vivo animal model. *J. Endourol.* **2011**, *25*, 1209–1215. [[CrossRef](#)] [[PubMed](#)]
18. Welch, A.J.; Van Gemert, M.J.C. *Optical-Thermal Response of Laser-Irradiated Tissue*; Plenum Press: New York, NY, USA, 1995; pp. 275–303.



© 2017 by the authors. Licensee MDPI, Basel, Switzerland. This article is an open access article distributed under the terms and conditions of the Creative Commons Attribution (CC BY) license (<http://creativecommons.org/licenses/by/4.0/>).